Redox Intermediates in the Catalase Cycle of Catalase-Peroxidases from *Synechocystis* PCC 6803, *Burkholderia pseudomallei,* and *Mycobacterium tuberculosis*†

Christa Jakopitsch,‡ Jutta Vlasits,‡ Ben Wiseman,§ Peter C. Loewen,§ and Christian Obinger*,‡

Department of Chemistry, Division of Biochemistry, BOKU-University of Natural Resources and Applied Life Sciences, Muthgasse 18, A-1190 Vienna, Austria, and Department of Microbiology, University of Manitoba, Winnipeg, MB R3T 2N2 Canada

Received November 2, 2006; Revised Manuscript Received December 8, 2006

ABSTRACT: Monofunctional catalases (EC 1.11.1.6) and catalase-peroxidases (KatGs, EC 1.11.1.7) have neither sequence nor structural homology, but both catalyze the dismutation of hydrogen peroxide ($2H_2O_2 \rightarrow 2H_2O + O_2$). In monofunctional catalases, the *catalatic* mechanism is well-characterized with conventional compound I [oxoiron(IV) porphyrin π-cation radical intermediate] being responsible for hydrogen peroxide oxidation. The reaction pathway in KatGs is not as clearly defined, and a comprehensive rapid kinetic and spectral analysis of the reactions of KatGs from three different sources (*Synechocystis* PCC 6803, *Burkholderia pseudomallei*, and *Mycobacterium tuberculosis*) with peroxoacetic acid and hydrogen peroxide has focused on the pathway. Independent of KatG, but dependent on pH, two low-spin forms dominated in the catalase cycle with absorbance maxima at 415, 545, and 580 nm at low pH and 418 and 520 nm at high pH. By contrast, oxidation of KatGs with peroxoacetic acid resulted in intermediates with different spectral features that also differed among the three KatGs. Following the rate of H_2O_2 degradation by stopped-flow allowed the linking of reaction intermediate species with substrate availability to confirm which species were actually present during the catalase cycle. Possible reaction intermediates involved in H_2O_2 dismutation by KatG are discussed.

All aerobically growing organisms have to deal with reactive oxygen species (ROSs), e.g., superoxide radicals, hydrogen peroxide, and hydroxyl radicals. Nature has evolved specialized enzymes for the degradation of the different ROSs to protect the cells. The obvious role of catalases is to dismutate hydrogen peroxide into water and oxygen. There is a high degree of diversity among *catalatically* active enzymes, and according to their primary and quaternary structure, subunit size, and prosthetic group, they have been divided into four subgroups: monofunctional heme *b*- or *d*-containing catalases, bifunctional heme *b*-containing catalase-peroxidases, nonheme catalases, and, finally, proteins with minor *catalatic* activity like monofunctional peroxidases (*1*). Here, we focus on the heme *b*-containing monofunctional catalases and catalase-peroxidases (KatGs).[1] Monofunctional catalases are found in all kingdoms of life, whereas KatGs are found only in archaea, bacteria, and fungi (*2*).

Although both types of heme enzymes exhibit high *catalatic* activities, there are significant differences, including the absence of any sequence homology and very different tertiary and quaternary structures, including the active site residues (Figure 1). The most highly conserved part in catalases is an eight-stranded antiparallel β-barrel domain with six α-helical insertions in the turns between the strands. The internal parts of this domain harbor essential distal side residues His74, Ser113, and Asn147 (BLC numbering) and the proximal heme iron ligand Tyr357 (*3*). In contrast, KatGs contain 20 α-helices per monomer, 10 in the N-terminal domain and 10 in the C-terminal domain organized in a manner very similar to that of other class I peroxidases (*4*, *5*). Heme is bound only to the N-terminal domain, and the function of the duplicated C-terminal domain is still under discussion (*6*). The active side residues include Arg108, His112, and Trp111 (BpKatG numbering) on the distal side of the heme and the proximal ligand His279 (Figure 1D). A covalent adduct involving Trp111, Tyr238 [situated on a loop not found in the other class I peroxidases but highly conserved in KatGs (*7*)], and Met264 has been shown to be essential for the *catalatic* activity of KatGs (*8*−*13*).

Catalase or peroxidase cycles are initiated by the H_2O_2-mediated oxidation of the native ferric enzyme to com-

† This work was supported by the Austrian Science Funds (FWF Project P18751). This work was also supported by grants from the Natural Sciences and Engineering Research Council of Canada (to P.C.L.) and by the Canadian Research Chair Program (to P.C.L.).

* To whom correspondence should be addressed. E-mail: christian.obinger@boku.ac.at. Phone: +43-1-36006-6073. Fax: +43-1-36006-6059.

‡ BOKU-University of Natural Resources and Applied Life Sciences.

§ University of Manitoba.

[1] Abbreviations: KatG, catalase-peroxidase; SynKatG, catalase-peroxidase from *Synechocystis* PCC 6803; BpKatG, catalase-peroxidase from *B. pseudomallei*; MtbKatG, catalase-peroxidase from *M. tuberculosis*; WT, wild-type; CCP, cytochrome *c* peroxidase; BLC, bovine liver catalase; PAA, peroxoacetic acid; mCPB, *m*-chloroperbenzoic acid; CT, charge transfer; EPR, electronic paramagnetic resonance; QM/MM, quantum mechanical/molecular mechanical.

10.1021/bi062266+ CCC: $37.00
Published on Web 01/13/2007

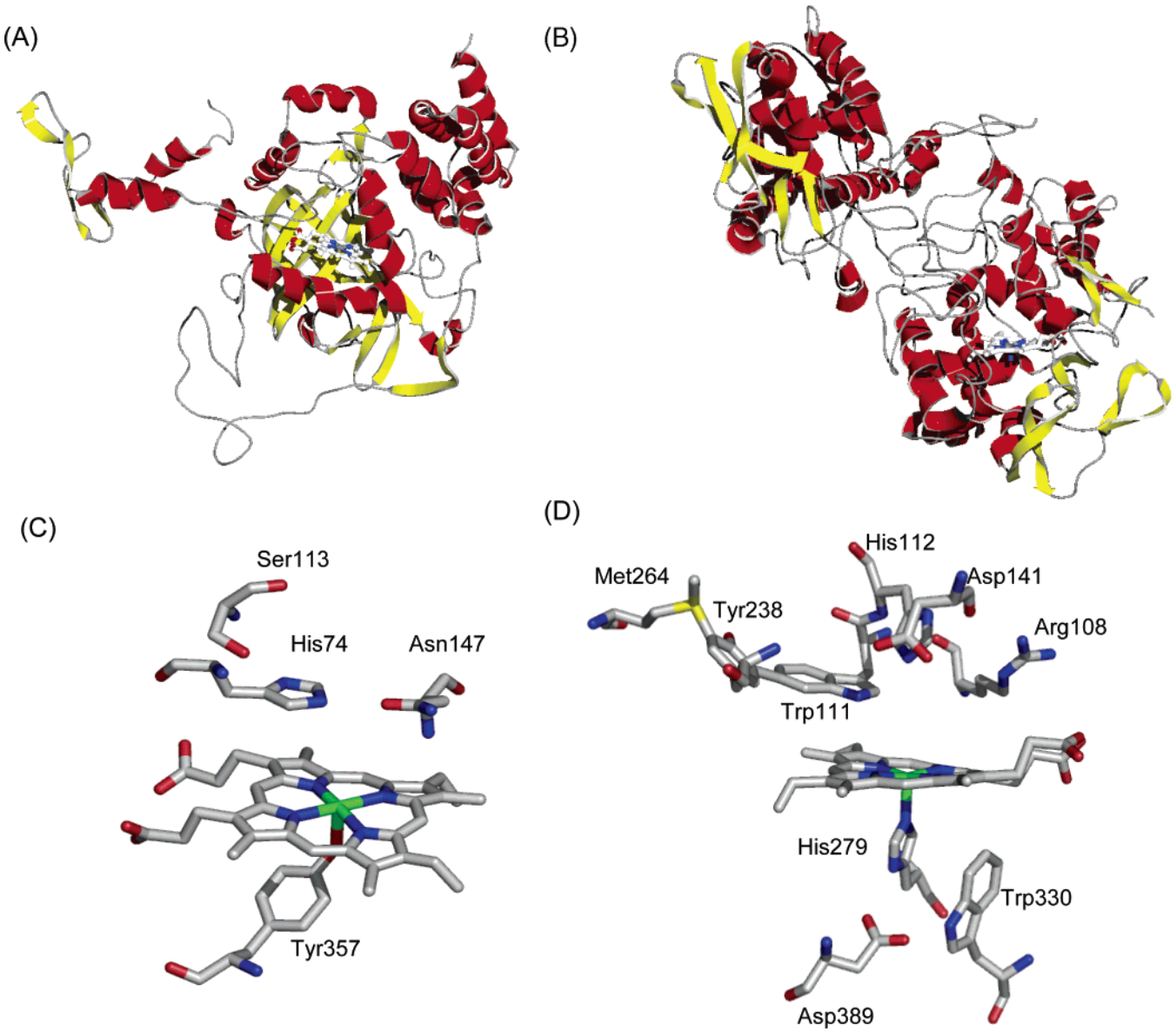

FIGURE 1: (A) Monomer of BLC (4BLC). (B) Monomer of KatG of *B. pseudomallei* (1MWV). (C) Active side residues in BLC. (D) Active side residues in KatG. The figures were constructed using the coordinates in the Protein Data Bank.

pound I. Generally, compound I is a redox intermediate two oxidizing equivalents above the resting state. This reaction causes the release of one water molecule and coordination of the second oxygen atom to the iron center (*14*, *15*). In monofunctional catalases, compound I is an oxoiron(IV) porphyrin π-cation radical species ($Por^{\bullet+}Fe^{IV}{=}O$) (*16*) which is reduced back to the ferric enzyme by a second molecule of hydrogen peroxide with the release of oxygen and water (*14*). In the reaction of BLC with peroxoacetic acid, a tyrosine radical can be formed by migration of an electron to the porphyrin π-cation radical. However, the high rate of turnover suggests that the tyrosyl radical plays no role in the *catalatic* reaction (*16*).

A lively debate about the *catalatic* mechanism in KatGs continues. Like that of BLC, reaction of KatGs with organic peroxides generates an oxoiron(IV) porphyrin π-cation radical species, which rapidly transforms to a protein radical species (*17*−*19*), but with spectral UV−vis signatures dissimilar to those described in monofunctional catalases and peroxidases (*1*, *8*−*11*). Because of the high intrinsic catalase activity generating molecular oxygen, it has been difficult to trap the spectroscopic signatures of the H_2O_2-generated *catalatic* intermediates. In this paper, we have used stopped-flow techniques to characterize the UV−vis signatures of the dominant *catalatic* intermediates of KatGs from three different sources (*Synechocystis* PCC 6803, *Mycobacterium tuberculosis*, and *Burkholderia pseudomallei*) at pH 5.6, 7.0, and 8.5 and to monitor H_2O_2 degradation under identical conditions. So far, almost all mechanistic studies have been conducted with these three enzymes, which share all KatG-typical structural features but also showed some differences in radical transformation when treated with organic peroxides (*17*−*19*). Significant differences in comparison to BLC are documented and discussed in terms of possible reaction schemes.

MATERIALS AND METHODS

Reagents. Standard chemicals and biochemicals of the highest available grade were obtained from Sigma. Hydrogen peroxide was from Sigma, and its concentration was deter-

mined using an extinction coefficient at 240 nm of 39.4 M^{-1} cm^{-1}. To eliminate H_2O_2 from commercial peroxoacetic acid (PAA), BLC (5 nM) was added to the buffered PAA stock solutions. BLC was obtained from Sigma and used without further purification. An extinction coefficient at 404 nm of 105 000 M^{-1} cm^{-1} was used for the determination of protein concentration. Recombinant catalase-peroxidase from *Synechocystis* was produced in *Escherichia coli* and purified as previously reported (*20*). *B. pseudomallei* and *M. tuberculosis* (Mtb) KatGs were produced and purified as previously described (*5*).

Steady-State Kinetics. Catalase activity was determined polarographically using a Clark-type electrode (YSI 5331 oxygen probe) inserted into a stirred thermostated water bath (YSI 5301B). To cover the pH range of 4.0−9.0, 50 mM citrate-phosphate, 50 mM phosphate, or 50 mM Tris-HCl buffer was used. All reactions were performed at 30 °C (37 °C in the case of BpKatG) and started by addition of KatG. One unit of catalase is defined as the amount that decomposes 1 μmol of H_2O_2/min at pH 7 and 25 °C.

Transient-State Kinetics. Transient-state measurements were taken using a model SX.18MV stopped-flow spectrophotometer and a PiStar-180 circular dichroism spectrometer (Applied Photophysics Ltd.) equipped with a 1 cm observation cell. Calculation of pseudo-first-order rate constants (k_{obs}) from experimental time traces was performed with a SpectraKinetic workstation (version 4.38) interfaced with the instrument. The substrate concentrations were at least 5 times that of the enzyme to allow determination of pseudo-first-order rate constants. Second-order rate constants were calculated from the slope of the linear plot of the pseudo-first-order rate constants versus substrate concentration. To follow spectral transitions, a model PD.1 photodiode array accessory (Applied Photophysics Ltd.) connected to the stopped-flow machine together with XScan diode array scanning software (version 1.07) was utilized. The kinetics of oxidation of ferric enzymes by hydrogen peroxide and organic peroxides were followed in the single mixing mode. The first data point was recorded 1.3 ms after mixing, and 2000 data points were accumulated. Sequential mixing stopped-flow analysis was used to assess compound I reduction (preformed with peroxoacetic acid) by hydrogen peroxide. In detail, 3 μM enzyme was mixed with 100−200 μM peroxoacetic acid (final concentration), and after a defined delay time, compound I was mixed with hydrogen peroxide. All stopped-flow measurements were taken at 25 °C, and at least three determinations were performed per substrate concentration.

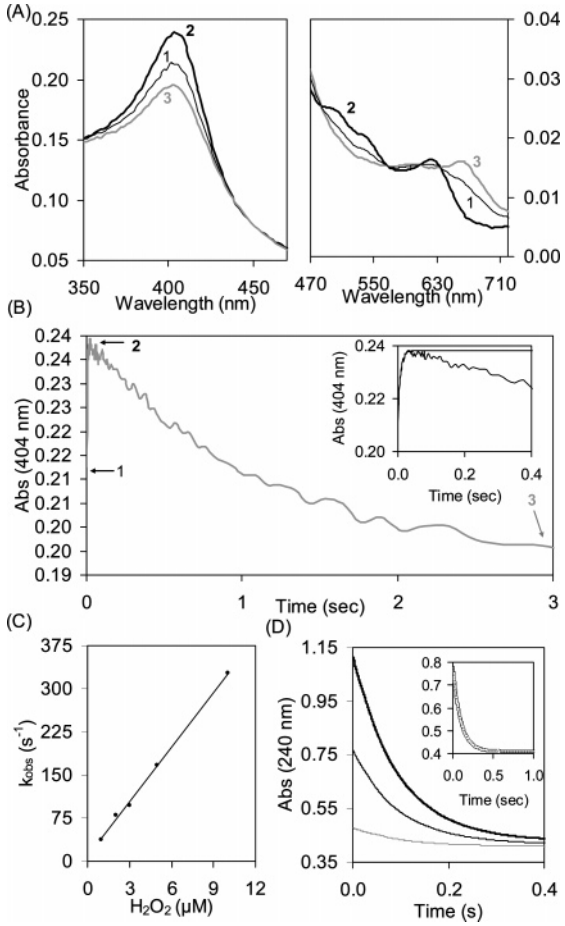

FIGURE 2: Reaction of BLC with peroxides. (A) Hydrogen peroxide-mediated reduction of BLC compound I preformed with 100 μM peroxoacetic acid. Spectral changes observed after addition of 10 μM hydrogen peroxide to 3 μM BLC compound I. Spectrum 1 is the first detectable spectrum (1.3 ms after compound I is mixed with H_2O_2). Spectrum 2 was taken 20 ms after mixing and dominated during H_2O_2 degradation. Finally, compound I was reformed due to the excess of peroxoacetic acid in the reaction mixture (spectrum 3, taken after 3 s). Conditions: 50 mM phosphate buffer at pH 7.0 and 25 °C. (B) Time trace followed at 404 nm for the reaction in panel A. Arrows indicate times of spectra selection. The inset shows the time trace including the single-exponential fit that reflects reduction of compound I by 10 μM hydrogen peroxide. (C) Plot of the pseudo-first-order rate constants for compound I reduction (k_{obs}) vs the concentration of H_2O_2. (D) Time traces of H_2O_2 degradation followed at 240 nm for the reaction of 2 μM ferric BLC with 2 mM (gray line), 10 mM (thin line), and 20 mM (thick line) hydrogen peroxide. Conditions: 50 mM phosphate buffer at pH 7.0 and 25 °C. The inset shows the time trace and single-exponential fit for the reaction of 2 μM BLC with 10 mM hydrogen peroxide.

RESULTS

Mechanism of the Reaction of BLC with Peroxides. In monofunctional catalases, the formation of an oxoiron(IV) porphyryl radical compound I ($Por^{\bullet+}Fe^{IV}=O$) cannot be followed spectroscopically using a moderate excess of hydrogen peroxide, because reduction of compound I by H_2O_2 (reaction 2) is faster than its formation (reaction 1).

$$PorFe^{III} + H_2O_2 \xrightarrow{k_1} Por^{\bullet+}Fe^{IV}=O + H_2O \quad (1)$$

$$Por^{\bullet+}Fe^{IV}=O + H_2O_2 \xrightarrow{k_2} PorFe^{III} + O_2 + H_2O \quad (2)$$

For comparison with KatGs, we revisited BLC to monitor the spectral features of intermediates formed during the reaction of the ferric enzyme with H_2O_2 and the kinetics of H_2O_2 degradation at 240 nm in the stopped-flow apparatus. As an example, a 2 μM solution of BLC depleted a 2 mM solution of H_2O_2 within 300 ms (Figure 2D). The time trace of H_2O_2 depletion can be exactly represented by a single-exponential equation (inset of Figure 2D). The spectral features that predominated during the reaction strongly resembled those of the ferric enzyme, consistent with a *catalatic* cycle of only reactions 1 and 2 where $k_2 > k_1$, as described in the literature (*1*). No red shift of the Soret band

or other features typical of a BLC compound I species were observed over the pH range of 5−10 (not shown).

In BLC and monofunctional heme *b* catalases, generally an oxoiron(IV) porphyryl radical compound I (characterized by a hypochromicity at the Soret region of 40−45% and a long wavelength band at 665−670 nm of an intensity almost equal to that of the original CT band of the ferric enyzme) is formed during reaction with peroxoacetic acid (*1*) (Figure 2A, spectrum 3). The reaction of preformed compound I with hydrogen peroxide (reaction 2) was followed in sequential-mixing mode, revealing that BLC compound I readily reacts with hydrogen peroxide directly to the ferric enzyme (Figure 2A), underlining the fact that the oxoiron(IV) porphyryl radical species indeed participates in the catalatic cycle and is responsible for the oxidation of H_2O_2 to O_2. Spectra 1 and 2 in Figure 2 recorded 1.3 and 20 ms, respectively, after mixing 10 μM H_2O_2 with 3 μM BLC compound I already resemble (15−20% hypochromicity) that of the ferric enzyme and did not change during H_2O_2 degradation. After complete H_2O_2 dismutation, the compound I spectrum reappeared as a result of reaction with excess peroxoacetic acid (spectrum 3, Figure 2). The time trace for reduction of compound I by hydrogen peroxide was fitted to a single-exponential equation, and the resulting linear plot of the pseudo-first-order rate constants versus H_2O_2 concentration (Figure 2C) produced a second-order rate constant (k_2) of 3.2×10^7 M^{-1} s^{-1} at pH 7.0, in good agreement with the value estimated by Chance (*21*).

Kinetics of Hydrogen Peroxide Degradation Mediated by Catalase-Peroxidases. A significant difference in the turnover rates of BLC and KatG is evident (compare Figures 2D and 3C), with 2 μM KatG from *Synechocystis* (SynKatG) degrading 10 mM hydrogen peroxide in ~1.4 s compared to 0.5 s for 2 μM BLC. Furthermore, the kinetics of degradation of H_2O_2 by KatG differed from those of BLC in that they could not be fitted to a single-exponential equation (Figure 3B−D). Similar results were obtained with KatGs from *M. tuberculosis* and *B. pseudomallei*.

To understand the differences in the shape of the time traces between BLC and KatG, it is advisable to describe the H_2O_2 dismutation reaction by a bi-uni mechanism similar to the reaction catalyzed by superoxide dismutase, SOD (i.e., dismutation of superoxide to hydrogen peroxide and oxygen). According to the mechanism described for SOD by Fee and Bull (*22*), the *catalatic* cycle could be described by two irreversible (an oxidative and a reductive) reactions, with E being the enzyme in its resting state and CI representing a compound I species irrespective of its electronic structure:

$$E + H_2O_2 \underset{k_{-1}}{\overset{k_1}{\rightleftharpoons}} [E{-}H_2O_2] \xrightarrow{k_2} CI + H_2O \qquad (3)$$

$$CI + H_2O_2 \underset{k_{-3}}{\overset{k_3}{\rightleftharpoons}} [CI{-}H_2O_2] \xrightarrow{k_4} E + O_2 + H_2O \qquad (4)$$

The steady-state equation can be obtained using the method of King and Altman as follows (*23*):

$$\frac{-d[H_2O_2]}{dt} = \frac{2(1/k_2 + 1/k_4)^{-1}[\text{catalase}][H_2O_2]}{\dfrac{(1/k_2 + 1/k_4)^{-1}}{\left(\dfrac{1}{\dfrac{k_1k_2}{k_{-1}+k_2}} + \dfrac{1}{\dfrac{k_3k_4}{k_{-3}+k_4}}\right)^{-1}} + [H_2O_2]}$$

The productive binding rates for the oxidative (k_o) and reductive (k_r) half-reactions can be formulated as

$$k_o = k_1[k_2(k_{-1} + k_2)]$$

$$k_r = k_3[k_4(k_{-3} + k_4)]$$

Substitution of these binding rates into the steady-state equation allows the expression of the turnover number (k_{cat}) and the apparent Michaelis−Menten constant, K_m:

$$k_{cat} = (1/k_2 + 1/k_4)^{-1}$$

$$K_m = \frac{(1/k_2 + 1/k_4)^{-1}}{(1/k_o + 1/k_r)^{-1}}$$

This leads to two limiting cases. (A) A K_m much greater than the H_2O_2 concentration corresponds to a second-order process and represents the binding of hydrogen peroxide. A pseudo-first-order degradation rate of H_2O_2 will be monitored at 240 nm. (B) A K_m much lower than the H_2O_2 concentration represents saturation of the enzyme. A zero-order degradation rate of H_2O_2 will be monitored at 240 nm.

An apparent K_m value for BLC has been determined to be 93 mM (*24*), but our studies are limited to concentrations of hydrogen peroxide up to only 20 mM, because of the increasing inaccuracy at absorbances in excess of 1 and the vigorous oxygen evolution in the reaction cell at higher concentrations. Therefore, in the case of BLC where $K_m \gg [H_2O_2]$, a pseudo-first-order reaction is expected and observed (Figure 2D). By contrast, the K_m values of KatGs are much lower [4.2 mM for SynKatG, 2.5 mM for MtbKatG (*8*), and 5.9 mM for BpKatG (*25*), all at pH 7]. As a consequence, the shape of the time traces depends on the H_2O_2 concentration, following almost pseudo-first-order kinetics at H_2O_2 concentrations below 1 mM (Figure 3A) and deviating from the single-exponential fit at 10 mM H_2O_2 (Figure 3B). At alkaline pH, however, the rate of depletion of H_2O_2 was nearly linear at low concentrations of hydrogen peroxide, and the apparent K_m values at pH 8.5 were determined to be 0.4 mM (SynKatG) at 30 °C and 0.22 mM (BpKatG) at 37 °C, fully compatible with the observed linearity of the time traces and the kinetic model proposed above. At pH 8.5 and 10 mM H_2O_2, it follows that $K_m \ll [H_2O_2]$, and the model predicts a reaction that follows zero-order kinetics, which is reflected by the experimental findings (Figure 3C). At acidic pH, the apparent K_m values are comparable to those determined at pH 7.0 (4.7 mM for SynKatG and 5.7 mM for BpKatG at pH 5.6) and the time traces for 10 mM H_2O_2 degradation were nonlinear (Figure 3D) and did not fit well to a single-exponential equation.

The plot of the rate of H_2O_2 degradation determined by stopped-flow against pH was similar in shape to a plot using rates obtained from polarographic measurements of oxygen

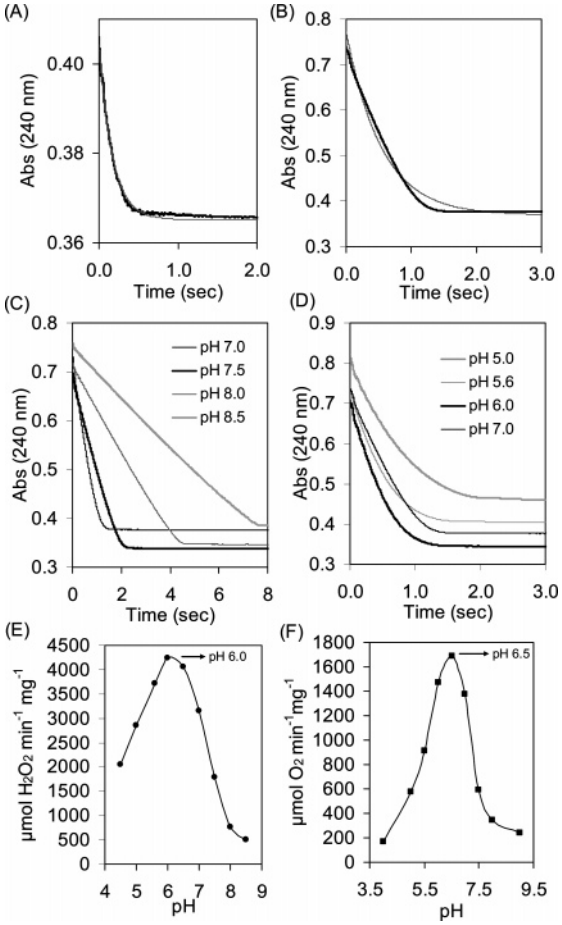

FIGURE 3: Kinetics of hydrogen peroxide degradation. (A) Time trace at 240 nm (black line) and single-exponential fit (gray line) for the reaction of 2 μM ferric wild-type KatG with 1 mM hydrogen peroxide. Conditions: 50 mM phosphate buffer at pH 7.0 and 25 °C. (B) Time trace (black line) and single-exponential fit (gray line) for the reaction of 2 μM ferric wild-type KatG with 10 mM hydrogen peroxide. Conditions as in panel A. (C) Time traces at 240 nm for the reaction of 2 μM ferric KatG with 10 mM hydrogen peroxide at pH 7.0, 7.5, 8, and 8.5. Conditions: 50 mM phosphate buffer at 25 °C. (D) Time traces at 240 nm for the reaction of 2 μM ferric KatG with 10 mM hydrogen peroxide at pH 5.0, 5.6, 6.0, and 7.0. Conditions: 50 mM phosphate buffers and 50 mM citrate/phosphate buffer at pH 5.0 and 25 °C. (E) pH dependence of hydrogen peroxide degradation determined by following H_2O_2 degradation at 240 nm in the stopped-flow apparatus. (F) pH dependence of oxygen evolution determined with a Clark-type electrode. Conditions: 50 mM citrate/phosphate buffers (pH 4.0−7.0) and 50 mM Tris-HCl buffers (pH 7.5−9.0) at 25 °C.

evolution (Figure 3E,F), but with maximum activity slightly shifted from pH 6.5 to 6.0. Similar results were obtained with MtbKatG and BpKatG, although the decrease in stopped-flow-determined activity in the acidic region was much more pronounced than in the polarographically determined rates. These small differences notwithstanding, the pH profiles of all KatGs exhibit a sharp optimum at pH 6−6.5, whereas BLC, and catalases in general, exhibit a broad pH optimum extending from pH 5.6 to 8.5 (not shown).

Reaction of Ferric Synechocystis KatG with Hydrogen Peroxide. A recently constructed variant of SynKatG, E253Q situated in the substrate entrance channel, has been found to slow the catalatic turnover sufficiently to allow the identification of spectral features of reaction intermediates in the catalase cycle (*26*). With a rate too rapid to be measured by

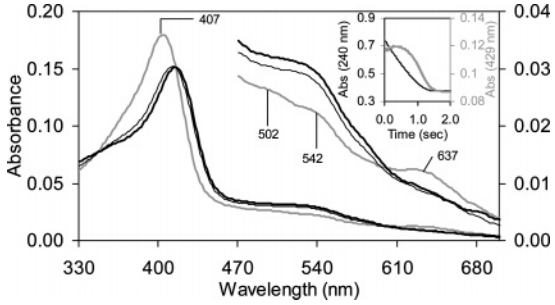

FIGURE 4: Reaction of wild-type *Synechocystis* KatG with hydrogen peroxide at pH 7.0. Spectra were recorded 1.3 ms after mixing of 2 μM ferric KatG (gray line) with 2 mM (thin line) and 20 mM (thick line) hydrogen peroxide. Conditions: 50 mM phosphate buffer at pH 7.0 and 25 °C. The inset shows the comparison of the time traces at 240 and 429 nm for the reaction of 2 μM ferric KatG with 10 mM hydrogen peroxide. Conditions: 50 mM phosphate buffer at pH 7.0 and 25 °C.

stopped-flow techniques, a 50-fold excess of H_2O_2 generated an intermediate exhibiting the spectral features of a low-spin species, including a red-shifted Soret band, hyperchromicity in the Q-band region (502 and 542 nm), formation of a broad shoulder around 520 nm, and disappearance of the high-spin CT band at 637 nm. Carrying out the same experiment with native SynKatG produced an intermediate with the same spectral features, but only at a much higher excess (at least 1000-fold) of H_2O_2, necessitated by the higher *catalatic* activity of native KatG compared to E253Q (Figure 4). Generally, increasing amounts of H_2O_2 caused an increasingly more pronounced red shift of the Soret band within 1.3 ms of mixing, and the reaction intermediate was evident only until all of the H_2O_2 was exhausted (inset of Figure 4). For example, after 1 s, the time needed to completely deplete 10 mM H_2O_2 with 2 μM SynKatG, the spectrum of ferric protein was recovered.

The pH dependence of the appearance of the reaction intermediate was directly related to the pH dependence of the *catalatic* reaction. At pH 8.5, the reaction is only 15% of the rate at pH 7, resulting in less H_2O_2 being necessary for the appearance of the spectral signatures of the intermediate (Figure 5A). No other spectral changes were evident even with a 1000-fold excess of H_2O_2 at pH 8.5 (Figure 5A). A different situation was observed at acidic pH (Figure 5B) where the first intermediate that could be trapped had spectral features completely different from those observed at pH 7.0 and 8.5. A 1000-fold excess of H_2O_2 within 1.3 ms generated a spectrum with a slightly decreased and red-shifted Soret band, and addition of even greater excesses (up to 100000-fold) caused a shift of the Soret band to 417 nm and the appearance of two distinct peaks at 545 and 578 nm (Figure 5B), reminiscent of the spectra of compound III of SynKatG (*27*), of the intermediate from the SynKatG variant Y249F mixed with a moderate excess of hydrogen peroxide (*9*), and of the alkaline forms of plant-type peroxidases ("Fe^{III}-OH") (*28*).

At intermediate pH 6.5, the first trapped spectrum exhibits a broad shoulder around 520 nm as well as a shoulder around 580 nm suggesting a mixture of the spectral signatures observed at pH 7.0 and 5.6 (Figure 5C). As the insets of panels A−C of Figure 5 indicate, there was a pH-dependent correlation between H_2O_2 degradation and the intermediate present. Analysis of spectra at pH 8.5 and 5.6 (Figure 6A,B)

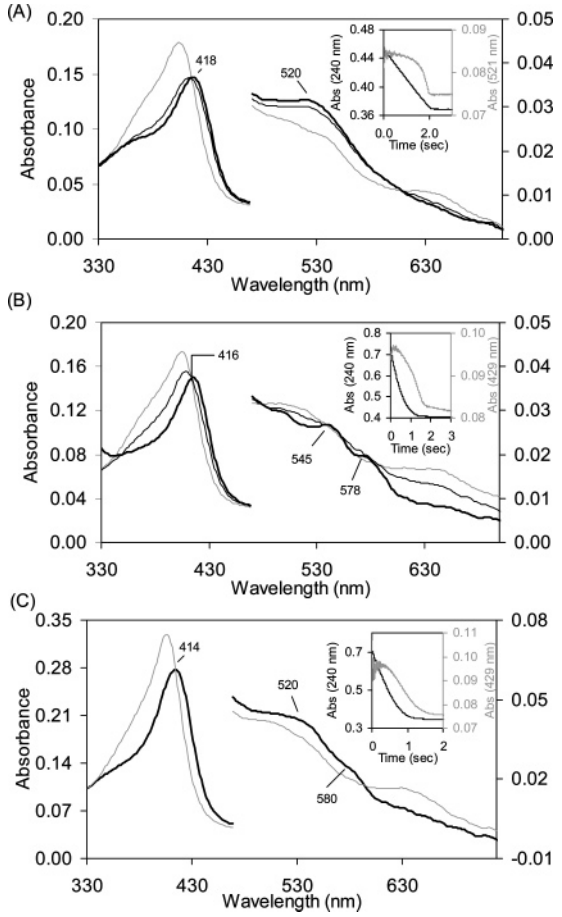

FIGURE 5: pH dependence of the reaction of ferric wild-type *Synechocystis* KatG with hydrogen peroxide. (A) Spectra recorded 1.3 ms after 2 μM ferric KatG (gray line) was mixed with 200 μM (thin line) and 2 mM (thick line) hydrogen peroxide at pH 8.5. Conditions: 50 mM phosphate buffer at pH 8.5 and 25 °C. The inset shows time traces at 240 nm (black line) and 521 nm (gray line) for the reaction of 2 μM wild-type KatG with 2 mM hydrogen peroxide at pH 8.5. (B) Spectra recorded 1.3 ms after 2 μM ferric KatG (gray line) was mixed with 2 mM (thin line) and 200 mM (thick line) hydrogen peroxide at pH 5.6. Conditions: 50 mM phosphate buffer at pH 5.6 and 25 °C. The inset shows time traces at 240 nm (black line) and 429 nm (gray line) for the reaction of 2 μM wild-type KatG with 10 mM hydrogen peroxide at pH 5.6. Conditions as in panel B. (C) Spectra recorded 1.3 ms after 3 μM ferric KatG (gray line) was mixed with 10 mM (thick line) hydrogen peroxide at pH 6.5. Conditions: 50 mM phosphate buffer at pH 6.5 and 25 °C. The inset shows time traces at 240 nm (black line) and 429 nm (gray line) for the reaction of 2 μM wild-type KatG with 10 mM hydrogen peroxide at pH 6.5. Conditions as in panel C.

in conjunction with the rates of H_2O_2 degradation (Figure 6C,D) reveals a single spectral signature (418 and 520 nm) at pH 8.5 throughout the H_2O_2 degradation phase and continuously changing spectra during advanced H_2O_2 depletion at pH 5.6 starting with a 1.3 ms spectrum with peaks at 415, 545, and 580 nm and ending with the Soret band at 407 nm and reappearance of the CT band at 637 nm.

Reaction of SynKatG Sequentially with Peroxoacetic Acid and H_2O_2. The oxidation of KatGs by peroxoacetic acid has been shown to give rise to a calculated reaction rate of $2-6 \times 10^4$ M^{-1} s^{-1}, depending on the source of KatG (*8*, *11*, *29*). The spectral signatures of the SynKatG compound I intermediate include a 40−50% hypochromicity of the Soret band and two distinct bands at 604 and 643 nm which were attributed to an oxoiron(IV) porphyrin radical cation species

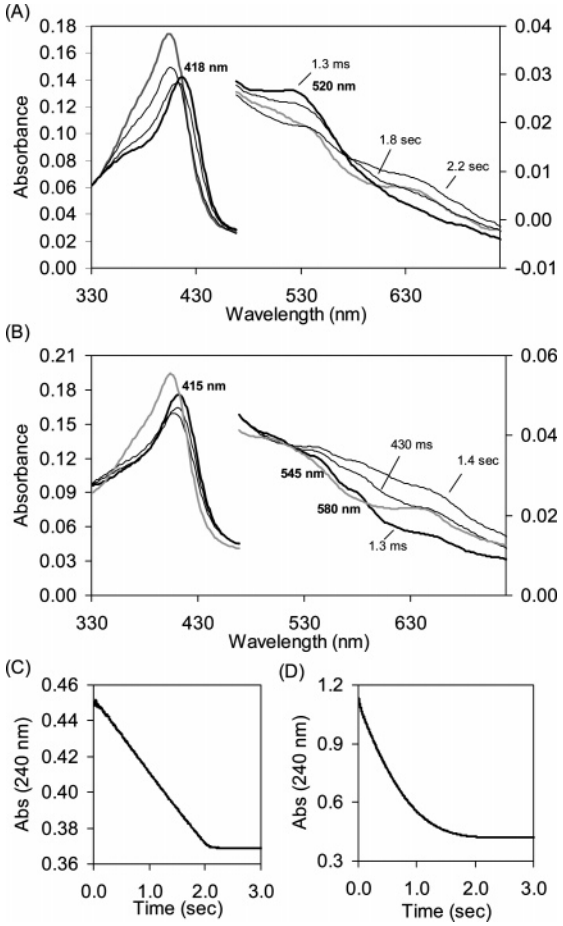

FIGURE 6: pH dependence of spectral transitions during hydrogen peroxide turnover of *Synechocystis* KatG. (A) Reaction of 2 μM KatG with 2 mM H_2O_2 at pH 8.5. The thick line is the spectrum 1.3 ms after mixing. This spectral signature persisted for 1.5 s. Subsequent spectra were taken after 1.8 s and after 2.2 s. For orientation, the spectrum of ferric KatG at pH 8.5 is colored gray. (B) Reaction of 2 μM KatG with 20 mM H_2O_2 at pH 5.6. The thick line is the spectrum observed 1.3 ms after mixing. Subsequent spectra were taken at 430 ms and 1.4 s. The gray line is the spectrum for ferric KatG at pH 5.6. (C) Hydrogen peroxide depletion recorded at 240 nm for the reaction in panel A. (D) Hydrogen peroxide depletion recorded at 240 nm for the reaction in panel B.

(*20*). No pH-dependent differences in the kinetics of its formation or its spectral properties were observed in the pH range of 5.6−8.5. EPR has demonstrated that upon reaction of SynKatG with peroxoacetic acid in the absence of electron donors, a $Por^{\bullet+}$ and, subsequently, two protein-based radicals, a $Trp^{\bullet}$ and a $Tyr^{\bullet}$, are formed (*10*).

In contrast to BLC, the compound I form of SynKatG produced by PAA did not appear to react readily with moderate levels of H_2O_2 back to the resting state. However, the addition of a large excess of hydrogen peroxide did cause a spectral transition, suggesting formation of the same intermediates that were formed in the direct reaction of ferric SynKatG with H_2O_2 (Figure 7A). For example, spectra recorded during the reaction of 3 μM SynKatG compound I with 6 mM hydrogen peroxide at pH 7.0 reveal a reaction intermediate with a Soret band at 418 nm, a broad shoulder at 520 nm, and no absorbance in the CT region while H_2O_2 degradation was taking place. Upon depletion of H_2O_2, the PAA-generated compound I reappeared, a result of the excess

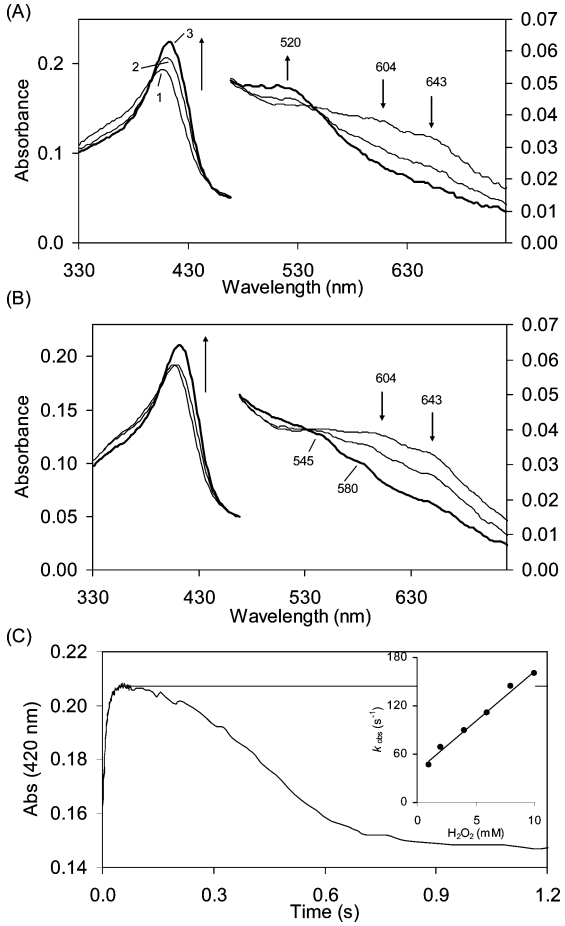

FIGURE 7: Reaction of hydrogen peroxide with *Synechocystis* KatG compound I preformed with peroxoacetic acid. (A) Spectral changes observed in the reaction of 3 μM WT KatG compound I with 6 mM hydrogen peroxide. Spectra were taken immediately after mixing (1.3 ms), after 15 ms, and after 50 ms. Conditions: 50 mM phosphate buffer at pH 7.0 and 25 °C. (B) Spectral changes upon mixing 3 μM WT KatG compound I with 10 mM hydrogen peroxide. The first spectrum is the compound I spectrum, and subsequent spectra were taken after 1.3 ms and after 20 ms. Conditions: 50 mM phosphate buffer at pH 6.0 and 25 °C. (C) Time trace at 420 nm and single-exponential fit for the reaction in panel A. The inset shows the plot of the pseudo-first-order rate constant vs the concentration of hydrogen peroxide.

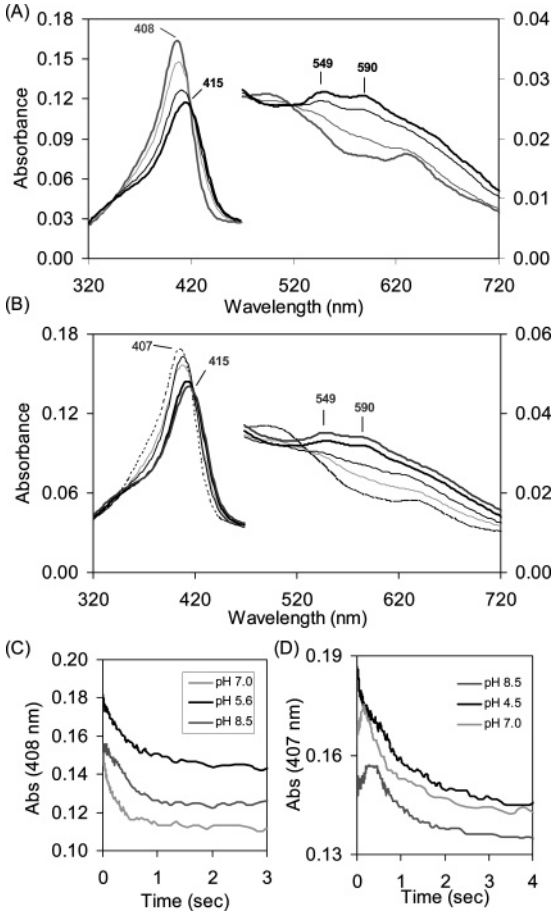

FIGURE 8: Reaction of *M. tuberculosis* and *B. pseudomallei* KatG with PAA. (A) Spectral changes observed upon mixing of 2 μM ferric *M. tuberculosis* KatG with 200 μM PAA. The thick gray line is for the ferric enzyme; subsequent spectra were taken after 1.3 ms (gray line), 220 ms (black line), and 1.1 s (thick black line). Conditions: 50 mM phosphate buffer at pH 7.0 and 25 °C. (B) Spectral changes observed upon mixing of 2 μM ferric *B. pseudomallei* KatG with 100 μM PAA. The dashed line is for the ferric enzyme; subsequent spectra were taken after 1.3 ms (gray line), 200 ms (black line), 1.9 s (thick black line), and 10 s (thick gray line). Conditions: 50 mM phosphate buffer at pH 7.0 and 25 °C. (C) pH dependence of compound I formation in *M. tuberculosis*. The time traces for the reaction of 2 μM ferric *M. tuberculosis* KatG with 200 μM PAA observed at 408 nm at various pH values are shown. (D) pH dependence of compound I formation in *B. pseudomallei*. The time traces for the reaction of 2 μM ferric *B. pseudomallei* KatG with 200 μM PAA observed at 407 nm at different pH values are shown.

PAA being in the reaction mixture (not shown). The time course of this reaction as reflected by hyperchromicity and a shift to 418 nm of the Soret band during the first 50 ms was monophasic (black line in Figure 7C) and could be fit to a single-exponential equation (gray line). Plotting these pseudo-first-order rate constants versus H_2O_2 concentration (inset of Figure 7C) yielded a second-order rate constant of 1.3×10^4 M^{-1} s^{-1}. The intercept of the plot was relatively high (38 s^{-1}) which reflected the fact that the formed intermediate was not a stable end product but subjected to permanent turnover during H_2O_2 degradation. At pH 8.5, the spectral transitions were similar to those at pH 7.0 (not shown), whereas at pH 6.0, the Soret band shifted to 416 nm which was accompanied by absorbance decreases at 604 and 643 nm and the appearance of peaks at 545 and 580 nm all following monophasic kinetics with a calculated rate constant of 1.5×10^4 M^{-1} s^{-1} (intercept of 12 s^{-1}) (Figure 7B).

Reaction of MtbKatG and BpKatG with Peroxoacetic Acid and H_2O_2. To compare the properties of SynKatG with those of other KatGs, MtbKatG and BpKatG were first treated with peroxoacetic acid, revealing spectral changes quite different from those observed in SynKatG, including a red-shifted Soret band (to 415 nm) and two new maxima around 549 and 590 nm (Figure 8A,B) that were stable for at least 10 s. At pH 7, the spectral changes of MtbKatG exhibit isosbestic points with a monophasic transition (Figure 8A), whereas the spectral changes of BpKatG were clearly not monophasic (Figure 8B). These spectra are similar to those previously reported for MtbKatG (*29*, *30*), but with a more red-shifted Soret band compared to the reported band at 411 nm (*29*, *30*), more prominent maxima at 549 and 590 nm, and a less intense shoulder at 655 nm (*29*). These spectral features varied only slightly over the pH range of 4.5−8.5 with a small increase in the magnitude of the 655 nm shoulder at higher pH.

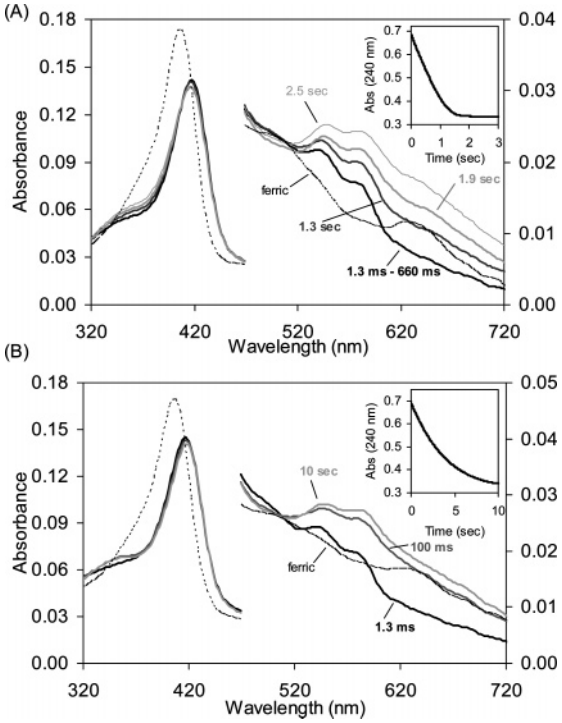

FIGURE 9: Reaction of *M. tuberculosis* KatG with hydrogen peroxide. (A) Spectral changes observed upon reaction of 2 μM *M. tuberculosis* KatG with 10 mM hydrogen peroxide at pH 7.0. Times at which spectra were taken are indicated (dashed line for the ferric enzyme). The inset shows the corresponding time trace for hydrogen peroxide degradation at 240 nm. Conditions: 50 mM phosphate buffer at pH 7.0 and 25 °C. (B) Spectral changes observed upon reaction of 2 μM *M. tuberculosis* KatG with 10 mM hydrogen peroxide at pH 5.6. The dashed line is for the ferric enzyme. The inset shows the corresponding time trace at 240 nm. Conditions: 50 mM phosphate buffer at pH 5.6 and 25 °C.

In contrast to SynKatG, the reactions of both MtbKatG and BpKatG with PAA were pH-dependent and the kinetics were not monophasic at all pH values. At both acidic and alkaline pHs, the reaction of MtbKatG with PAA was biphasic and slower than at pH 7 (Figure 8C). The kinetics of oxidation of BpKatG by PAA were slower than for MtbKatG, revealing greater complexity, including an initial hypochromicity of the Soret band at 407 nm followed by an increase in absorbance and red shift to 415 nm (Figure 8D). The time trace of the changes at 407 nm in combination with the other spectral transitions suggests the existence of a transient intermediate in the reaction pathway leading to the compound I species with the observed spectral features.

Mixing of MtbKatG and BpKatG with H_2O_2 at pH 8.5 produced intermediates with the same spectral features that were observed for SynKatG at pH 8.5 and 7.0 (418 and 520 nm) for as long as H_2O_2 was being degraded (data not shown). At pH 7.0, mixing of both MtbKatG and BpKatG with H_2O_2 gave rise to spectra very similar to that of SynKatG at pH 5.6 (Figure 9A). For example, the reaction of 2 μM MtbKatG with 10 mM hydrogen peroxide at pH 7.0 caused, within 1.3 ms and lasting for 600 ms, a red shift of the Soret band (416 nm), the appearance of two peaks around 545 and 580 nm, and a diminished CT1 band. Ultimately, the absorbance increased generally without a change in the position of the maxima at 416, 545, and 580 nm, and even after depletion of 10 mM H_2O_2 (1.8 s; see the inset of Figure 9A), these spectral features persisted (Figure 9A, spectra taken after 2.5 s). The reaction of ferric MtbKatG with H_2O_2 at pH 5.6 led to spectral changes similar to those observed at pH 7.0 (Figure 9B), except that the general increase in absorbance occurred faster (within 100 ms). After complete dismutation of H_2O_2, the spectrum remained almost identical to that resulting from PAA-mediated oxidation of MtbKatG (415, 549, and 590 nm). Similar results were obtained with BpKatG.

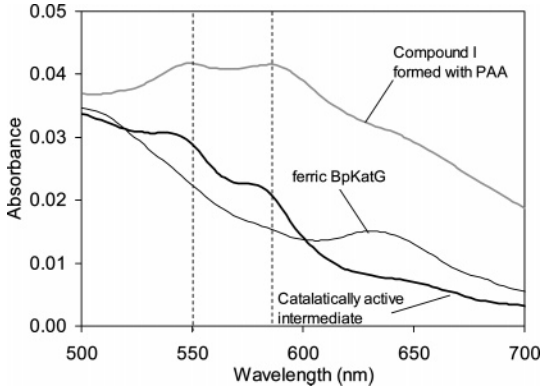

FIGURE 10: Spectral features of redox intermediates in BpKatG at pH 6.5. The black line is for 3 μM ferric BpKatG, the bold gray line for compound I obtained upon mixing of 3 μM ferric BpKatG with 200 μM PAA (final concentrations), and the thick black line for the intermediate formed upon addition of 50 mM hydrogen peroxide to compound I preformed with PAA. Conditions: 50 mM phosphate buffer at pH 6.5 and 25 °C.

Compared to that of SynKatG, the degradation of hydrogen peroxide by both MtbKatG and BpKatG was slower at pH 5.6, taking 10 s to dismutate 10 mM H_2O_2 compared to 2 s for SynKatG. The reaction of BpKatG with H_2O_2 was also tested at pH 4.5, made possible by its greater resistance to acidic conditions compared to SynKatG. A pH of 4.5 is the pH optimum for the peroxidase activity in BpKatG, and catalase activity is decreased to 30−40% of maximum levels at pH 6.5 but still higher than at pH 8.5 (*31*). The resulting spectral features of the intermediate were similar to those observed at pH 5.6 and 7.0 (415, 548, and 580 nm), but the reaction was slower with the spectrum at 1.3 ms, suggesting a mixture of the ferric enzyme and the intermediate. The reaction followed pseudo-first-order kinetics, and the bimolecular rate constant determined at a single concentration of hydrogen peroxide (1 mM) was 1.3×10^4 M^{-1} s^{-1}.

The final step was to investigate the reaction of compound I of BpKatG, generated using PAA, with H_2O_2. No spectral changes were observed using a moderate excess of H_2O_2, but a large excess (1000-fold range) resulted in the formation of intermediates with the same spectral features and pH dependence (Figure 10) as those formed in the direct mixing of the ferric protein with hydrogen peroxide (Figure 9). The transition between the spectral features of PAA-generated compound I of BpKatG and the spectral features of the intermediate dominating in the presence of H_2O_2 could be fitted to a single-exponential equation which yielded a second-order rate constant of 1.7×10^4 M^{-1} s^{-1} at both pH 6.5 and 8.5.

DISCUSSION

Despite catalyzing the same reaction ($2H_2O_2 \rightarrow 2H_2O + O_2$), heme-containing monofunctional catalases and bifunctional catalase-peroxidases do not share sequence or structural

similarities, raising the question of whether the reaction pathways are similar or different. Whereas catalases have been the subject of study for decades, the interest in catalase-peroxidases has developed more recently, in part because of its role in mediating isoniazid resistance in *M. tuberculosis*, but also from the standpoint of determining how an enzyme which so closely resembles a class I peroxidase can dismutate H_2O_2 at reasonable rates. The determination of crystal structures of KatGs, now from four different organisms, has led to the identification of several catalase-specific residues, subsequently confirmed by site-directed mutagenesis studies. Such unique features have suggested a number of unusual mechanisms controlling the catalase reaction, but a clear picture of the reaction pathway has remained elusive. To address this question, a comprehensive kinetic and spectral investigation of the reaction of three different catalase-peroxidases and one monofunctional catalase with H_2O_2 and PAA using stopped-flow techniques has been carried out and correlated with the kinetics of H_2O_2 degradation also monitored by stopped-flow spectroscopy.

The rate of H_2O_2 degradation by BLC is much faster than the rate exhibited by KatGs, but in both cases, the kinetics can be explained by a simple reaction pathway involving reactions 3 and 4. Changing the H_2O_2 concentration in the assay from below to higher than the apparent K_m of KatGs caused a change in the kinetic pattern of H_2O_2 degradation consistent with the change from a substrate-unsaturated to substrate-saturated state. Unfortunately, it was technically not possible to raise the H_2O_2 concentration above the apparent K_m for monofunctional catalases in the stopped-flow system to determine if they responded similarly. However, the overall reaction pathway involving H_2O_2 binding provides a reasonable explanation for the kinetic responses of the two enzymes. On the other hand, the very different pH profiles of the two classes of enzymes suggest some fundamental differences.

These differences are also evident in the spectral features of reaction intermediates formed during H_2O_2 dismutation by the two classes of enzymes which differ significantly. Two oxidized products have been observed after reaction of BLC with peroxoacetic acid, an oxoferryl prophyrin radical species and a presumed hydroxoferryl protein radical species (*1*, *16*). Neither of these species is evident in the reaction with H_2O_2 because the rate of reaction 2 is so much faster than the rate of reaction 1 that compound I does not accumulate. However, compound I preformed with peroxoacetic acid is reduced to the ferric state by H_2O_2 at a rapid rate, confirming that it is an intermediate in the catalatic pathway.

The much slower turnover rate for the catalatic reaction in KatGs compared to monofunctional catalases suggested that it might be possible to capture and characterize reaction intermediates of KatG with H_2O_2. This proved to be the case with the rapid appearance, within 1.3 ms of mixing H_2O_2 with enzyme, of the spectral signatures of two low-spin species that are different from the spectra of the compound I species of both BLC and KatG generated by peroxoacetic acid. Specifically, at pH 8.5, the spectra exhibited maxima at 418 and 520 nm, while at pH 5.6, the spectra exhibited maxima at 415, 545, and 580 nm; both spectra had lost the CT1 band at 640 nm. The relative proportions of the two intermediates varied at intermediate pHs, depending on the pH and the KatG. Maximal conversion of the enzyme into the reaction intermediate required saturation of the enzyme with substrate ($[H_2O_2]$ > apparent K_m).

The spectrum with features at 418 and 520 nm does not resemble the spectrum of any reaction intermediate previously reported in peroxidases or catalases. On the other hand, the spectrum with features at 415, 545, and 580 nm of the intermediate predominating at acidic pH resembles the spectra of compound III of plant peroxidases (*32*), the ferrous form of WT and the Y249F variant of SynKatG treated with O_2 (*27*), the ferric form of MtbKatG treated with superoxide (*33*), compound II of MtbKatG treated with excess H_2O_2 (*13*), the Y238F variant of BpKatG treated with peroxoacetic acid (unpublished data), several KatG variants treated with a small excess of H_2O_2 (*8*, *9*, *13*), HRP (*28*) [but not MtKatG (*34*)] at alkaline pH with a hydroxyl ion distal ligand, *Arthromyces ramosus* peroxidase with NH_2OH bound (*35*), and finally, to some extent, the inactive N-terminal domain of KatG of *E. coli* (416, 536, and 568 nm) (*36*). In the latter case, incubation of the N-terminal domain with a separately expressed C-terminal domain resulted in a partial restoration of both catalase and peroxidase activities as well as high-spin spectral features of wild-type KatG (*6*). In the case of the NH_2OH complex with the peroxidase, the crystal structure of the complex suggests coordination of the nitrogen atom to the heme iron and hydrogen bonding of the hydroxyl group with the distal histidine possibly representative of compound "0" or the H_2O_2−peroxidase complex prior to the reaction (*35*). The conclusion here should be that compound III-like spectra are not uncommon and may be exhibited by different six-coordinate low-spin structures.

The crystal structures of a number of catalase, peroxidase, and catalase-peroxidase peroxoacetic acid-generated reaction intermediates have recently been reported that reveal Fe−O bond lengths longer than the value of 1.65 Å expected for a classical compound I ($Por^{\bullet+}Fe^{IV}$=O) structure. *Micrococcus lysodeikticus* catalase (*37*), *Helicobacter pylori* catalase (2IQF, manuscript in review), CCP (*38*), and BpKatG (*39*) were converted to intermediates with Fe−O bond lengths of 1.82, 1.85, 1.87, and 1.93 Å, respectively. In all cases, the longer length was explained in terms of a $PorFe^{IV}$−OH species formed by a transfer of an electron from the protein to the porphyryl radical, and this has been corroborated in recent QM/MM calculations (*40*). Unfortunately, the situation has been complicated somewhat by QM and QM/MM calculations that postulate the existence of six isomers of horseradish peroxidase compound II, of which the two experimentally observed reaction intermediates, Fe^{IV}=O and Fe^{IV}−OH, are the least stable while the singlet and triplet states of the $Por^{\bullet+}Fe^{III}$−OH and $Por^{\bullet+}Fe^{III}$−OH_2 complexes are more stable (*41*).

EPR studies have revealed a number of radical-based reaction intermediates that are formed during the treatment of catalases, peroxidases, and catalase-peroxidases with peroxoacetic acid or H_2O_2. The classic compound I species has a radical on the porphyrin, a result of a one-electron transfer to the iron ($PorFe^{V}$=O → $Por^{\bullet+}Fe^{IV}$=O). This has been observed in virtually all heme peroxidases and catalases. However, specific enzymes in all classes also support the migration of an electron from the protein into the heme, quenching the porphyrin radical and producing a protein radical based on either a Trp or Tyr residue (*10*, *16*−*19*,

32). In such cases, protonation of the oxoferryl to form a hydroxoferryl species occurs rapidly ($PorFe^{IV}{=}O + H^+ \rightarrow PorFe^{IV}{-}OH$). In SynKatG, W106 has been identified as the site of a $Trp^{\bullet+}$ radical while the location of the $Tyr^{\bullet}$ remains unidentified. The diversity of radical sites even in the same class of enzymes is evident in the identification of the surface-situated Y353 as a radical site in MtKatG (*42*). Specific tyrosines have been identified as radical sites in CCP and lignin peroxidase (*32*).

The proximity of the KatG-specific adduct (MYW) to the reaction center stacked just 3.4 Å above the heme has led to conjecture about its role in the reaction. One proposal is that it forms one component of a molecular switch inductively controlling the catalase reaction (*39*). Arg426 can adopt two conformations depending on the pH and the oxidation state of the heme (*39*). In the Y conformation favored at pH >6.5, Arg429 is in ionic association with the adduct. Conformation Y is in equilibrium with conformation R, which is favored at pH <6.5 and predominates in KatG oxidized by PAA. Formation of an adduct radical as an intermediate during MYW formation has been proposed (*30*), but no radical has so far been experimentally associated with the adduct in EPR studies. This suggests that if an adduct radical is formed during catalysis, it is transient or short-lived, and freeze-quench EPR techniques will be required for its identification. Furthermore, the fact that the adduct is required for the catalase but not the peroxidase reaction suggests that if a transient radical on the adduct ($MYW^{\bullet+}$) is formed, it has a role only in the second stage of the catalase reaction, i.e., H_2O_2 oxidation, and not in the formation of compound I or the associated electron transfer pathway leading to protein radical formation (*10*, *13*). Alternative radical sites close to the heme, such as the proximal tryptophan observed in CCP (*43*), might also be considered.

In all of this, Arg426 plays a key role. On the one hand, its association with the tyrosinate ion on the adduct is required for optimal catalatic rates (*10*, *39*). The role of the putative adduct radical becomes complicated as a result, because removal of an electron from the adduct during radical formation would reduce the negative charge on the adduct, thereby weakening its association with Arg426. Therefore, quenching of the adduct radical to re-form the tyrosinate ion followed by its reassociation with Arg426 must either be a concerted part of or precede compound I reduction. Second, the change between the 415, 545, and 580 nm (low pH) and 418 and 520 nm (high pH) species with a midpoint around pH 6.5 correlates well with the 50:50 mixture of R and Y conformations of the Arg426 side chain at pH 6.5 (*44*). The influence of Arg426 on the predominant reaction intermediate could be a result of inductive stabilization of a particular intermediate or even the selection of alternate reaction pathways.

In light of the foregoing, a number of schemes can be envisioned that provide possible identities to the intermediates responsible for the previously unknown 418 and 520 nm and compound III-like 415, 545, and 580 nm intermediates. They range from the relatively simple compound I−substrate complex ($Por^{\bullet+}Fe^{IV}{=}O{-}H_2O_2$) to alternative compound I species that are active in H_2O_2 oxidation (reaction 4) and have the porphyryl radical quenched by an electron from the adduct ($MYW^{\bullet+}PorFe^{IV}{-}OH$), an alternative amino acid near the heme ($AA^{\bullet+}PorFe^{IV}{-}OH$), or both ($MYW^{\bullet+}PorFe^{III}{-}OH{-}AA^{\bullet+}$). Alternatively, because KatG is a class I peroxidase, it might utilize the modified catalatic mechanism of monofunctional peroxidases that includes formation of compound III ($PorFe^{II}{-}O_2 \leftrightarrows PorFe^{III}{-}O_2^{\bullet-}$) (*32*). In peroxidases, the slow decay of compound III is responsible for the low rate of catalatic turnover, but in KatG, a nearby radical located on the adduct (or an alternative site) [$MYW^{\bullet+}(AA^{\bullet+})PorFe^{II}{-}O_2 \leftrightarrows MYW^{\bullet+}(AA^{\bullet+})PorFe^{III}{-}O_2^{\bullet-}$] guarantees both a high turnover rate and the release of molecular oxygen. In any case, the pH-dependent change in the reaction intermediate can be explained by simple protonation and/or deprotonation of several intermediates or, alternatively, by different intermediates being stabilized at different pHs.

In summary, spectra suggestive of two different reaction intermediates, depending on pH, appear after KatGs are mixed with H_2O_2. One of the intermediates has not been reported previously, and it is clearly different from the signatures of intermediates generated after peroxoacetic acid treatment. Alternative techniques, including possibly freeze-quench EPR and Mössbauer spectroscopy, will have to be applied to differentiate among the possibilities.

REFERENCES

1. Nicholls, P., Fita, I., and Loewen, P. C. (2001) Enzymology and structure of catalases, *Adv. Inorg. Chem. 51*, 51−106.
2. Klotz, M. G., and Loewen, P. C. (2003) The molecular evolution of catalatic hydroperoxidases: Evidence for multiple lateral transfer of genes between prokaryota and from bacteria into eukaryota, *Mol. Biol. Evol. 20*, 1098−1112.
3. Ko, T. P., Day, J., Malkin, A. J., and McPherson, A. (1999) Structure of orthorhombic crystals of beef liver catalase, *Acta Crystallogr. D55*, 1383−1394.
4. Yamada, Y., Fujiwara, T., Sato, T., Igarashi, N., and Tanaka, N. (2002) The 2.0 Å crystal structure of catalase-peroxidase from *Haloarcula marismortui*, *Nat. Struct. Biol. 9*, 691−695.
5. Carpena, X., Loprasert, S., Mongkolsuk, S., Switala, J., Loewen, P. C., and Fita, I. (2003) Catalase-peroxidase KatG of *Burkholderia pseudomallei* at 1.7 Å resolution, *J. Mol. Biol. 327*, 475−489.
6. Baker, R. D., Cook, C. O., and Goodwin, D. C. (2006) Catalase-peroxidase active site restructuring by a distant and "inactive" domain, *Biochemistry 45*, 7113−7121.
7. Zamocky, M., Regelsberger, G., Jakopitsch, C., and Obinger, C. (2001) The molecular peculiarities of catalase-peroxidases, *FEBS Lett. 492*, 177−182.
8. Ghiladi, R. A., Knudsen, G. M., Medzihradszky, K. F., and de Montellano, P. R. (2005) The Met-Tyr-Trp cross-link in *Mycobacterium tuberculosis* catalase-peroxidase (KatG): Autocatalytic formation and effect on enzyme catalysis and spectroscopic properties, *J. Biol. Chem. 280*, 22651−22663.
9. Jakopitsch, C., Auer, M., Ivancich, A., Ruker, F., Furtmuller, P. G., and Obinger, C. (2003) Total conversion of bifunctional catalase-peroxidase (KatG) to monofunctional peroxidase by exchange of a conserved distal side tyrosine, *J. Biol. Chem. 278*, 20185−20191.
10. Jakopitsch, C., Ivancich, A., Schmuckenschlager, F., Wanasinghe, A., Poltl, G., Furtmuller, P. G., Ruker, F., and Obinger, C. (2004) Influence of the unusual covalent adduct on the kinetics and formation of radical intermediates in *Synechocystis* catalase peroxidase: A stopped-flow and EPR characterization of the MET275, TYR249, and ARG439 variants, *J. Biol. Chem. 279*, 46082−46095.
11. Regelsberger, G., Jakopitsch, C., Ruker, F., Krois, D., Peschek, G. A., and Obinger, C. (2000) Effect of distal cavity mutations on the formation of compound I in catalase-peroxidases, *J. Biol. Chem. 275*, 22854−22861.
12. Hillar, A., Peters, B., Pauls, R., Loboda, A., Zhang, H., Mauk, A. G., and Loewen, P. C. (2000) Modulation of the activities of catalase-peroxidase HPI of *Escherichia coli* by site-directed mutagenesis, *Biochemistry 39*, 5868−5875.

13. Yu, S., Girotto, S., Zhao, X., and Magliozzo, R. S. (2003) Rapid formation of compound II and a tyrosyl radical in the Y229F mutant of *Mycobacterium tuberculosis* catalase-peroxidase disrupts catalase but not peroxidase function, *J. Biol. Chem. 278*, 44121−44127.
14. Schonbaum, G. R., and Chance, B. (1976) in *The Enzymes*, Vol. 13, Academic Press, New York.
15. Fita, I., and Rossmann, M. G. (1985) The active center of catalase, *J. Mol. Biol. 185*, 21−37.
16. Ivancich, A., Jouve, H. M., Sartor, B., and Gaillard, J. (1997) EPR investigation of compound I in *Proteus mirabilis* and bovine liver catalases: Formation of porphyrin and tyrosyl radical intermediates, *Biochemistry 36*, 9356−9364.
17. Ivancich, A., Jakopitsch, C., Auer, M., Un, S., and Obinger, C. (2003) Protein-based radicals in the catalase-peroxidase of *Synechocystis* PCC6803: A multifrequency EPR investigation of wild-type and variants on the environment of the heme active site, *J. Am. Chem. Soc. 125*, 14093−14102.
18. Jakopitsch, C., Obinger, C., Un, S., and Ivancich, A. (2006) Identification of Trp106 as the tryptophanyl radical intermediate in *Synechocystis* PCC6803 catalase-peroxidase by multifrequency electron paramagnetic resonance spectroscopy, *J. Inorg. Biochem. 100*, 1091−1099.
19. Chouchane, S., Girotto, S., Yu, S., and Magliozzo, R. S. (2002) Identification and characterization of tyrosyl radical formation in *Mycobacterium tuberculosis* catalase-peroxidase (KatG), *J. Biol. Chem. 277*, 42633−42638.
20. Jakopitsch, C., Ruker, F., Regelsberger, G., Dockal, M., Peschek, G. A., and Obinger, C. (1999) Catalase-peroxidase from the cyanobacterium *Synechocystis* PCC 6803: Cloning, overexpression in *Escherichia coli*, and kinetic characterization, *Biol. Chem. 380*, 1087−1096.
21. Chance, B. (1949) The Primary and Secondary Compounds of Catalase and Methyl or Ethyl Hydrogen Peroxide. IV. Reactions with Hydrogen Peroxide, *J. Biol. Chem. 180*, 947−959.
22. Fee, J. A., and Bull, C. (1986) Steady-state kinetic studies of superoxide dismutases. Saturative behavior of the copper- and zinc-containing protein, *J. Biol. Chem. 261*, 13000−13005.
23. Segel, I. H. (1975) *Enyzme Kinetics*, Wiley-Interscience, New York.
24. Switala, J., and Loewen, P. C. (2002) Diversity of properties among catalases, *Arch. Biochem. Biophys. 401*, 145−154.
25. Deemagarn, T., Carpena, X., Singh, R., Wiseman, B., Fita, I., and Loewen, P. C. (2005) Structural characterization of the Ser324Thr variant of the catalase-peroxidase (KatG) from *Burkholderia pseudomallei*, *J. Mol. Biol. 345*, 21−28.
26. Jakopitsch, C., Droghetti, E., Schmuckenschlager, F., Furtmuller, P. G., Smulevich, G., and Obinger, C. (2005) Role of the main access channel of catalase-peroxidase in catalysis, *J. Biol. Chem. 280*, 42411−42422.
27. Jakopitsch, C., Wanasinghe, A., Jantschko, W., Furtmuller, P. G., and Obinger, C. (2005) Kinetics of interconversion of ferrous enzymes, compound II and compound III, of wild-type *Synechocystis* catalase-peroxidase and Y249F: Proposal for the catalatic mechanism, *J. Biol. Chem. 280*, 9037−9042.
28. Howes, B. D., Rodriguez-Lopez, J. N., Smith, A. T., and Smulevich, G. (1997) Mutation of distal residues of horseradish peroxidase: Influence on substrate binding and cavity properties, *Biochemistry 36*, 1532−1543.
29. Chouchane, S., Lippai, I., and Magliozzo, R. S. (2000) Catalase-peroxidase (*Mycobacterium tuberculosis* KatG) catalysis and isoniazid activation, *Biochemistry 39*, 9975−9983.
30. Ghiladi, R. A., Medzihradszky, K. F., and Ortiz de Montellano, P. R. (2005) Role of the Met-Tyr-Trp cross-link in *Mycobacterium tuberculosis* catalase-peroxidase (KatG) as revealed by KatG-(M255I), *Biochemistry 44*, 15093−15105.
31. Singh, R., Wiseman, B., Deemagarn, T., Donald, L. J., Duckworth, H. W., Carpena, X., Fita, I., and Loewen, P. C. (2004) Catalase-peroxidases (KatG) exhibit NADH oxidase activity, *J. Biol. Chem. 279*, 43098−43106.
32. Dunford, H. B. (1999) *Heme Peroxidases*, Wiley-VCH, New York.
33. Ghiladi, R. A., Cabelli, D. E., and Ortiz de Montellano, P. R. (2004) Superoxide reactivity of KatG: Insights into isoniazid resistance pathways in TB, *J. Am. Chem. Soc. 126*, 4772−4773.
34. Chouchane, S., Girotto, S., Kapetanaki, S., Schelvis, J. P., Yu, S., and Magliozzo, R. S. (2003) Analysis of Heme Structural Heterogeneity in *Mycobacterium tuberculosis* Catalase-Peroxidase (KatG), *J. Biol. Chem. 278*, 8154−8162.
35. Wariishi, H., Nonaka, D., Johjima, T., Nakamura, N., Naruta, Y., Kubo, S., and Fukuyama, K. (2000) Direct binding of hydroxylamine to the heme iron of *Arthromyces ramosus* peroxidase. Substrate analogue that inhibits compound I formation in a competetive manner, *J. Biol. Chem. 275*, 32919−32924.
36. Baker, R. D., Cook, C. O., and Goodwin, D. C. (2004) Properties of catalase-peroxidase lacking its C-terminal domain, *Biochem. Biophys. Res. Commun. 320*, 833−839.
37. Murshudov, G. N., Grebenko, A. I., Brannigan, J. A., Antson, A. A., Barynin, V. V., Dodson, G. G., Dauter, Z., Wilson, K. S., and Melik-Adamyan, W. R. (2002) The structures of *Micrococcus lysodeikticus* catalase, its ferryl intermediate (compound II) and NADPH complex, *Acta Crystallogr. D58*, 1972−1982.
38. Bonagura, C. A., Bhaskar, B., Shimizu, H., Li, H., Sundaramoorthy, M., McRee, D. E., Goodin, D. B., and Poulos, T. L. (2003) High-resolution crystal structures and spectroscopy of native and compound I cytochrome c peroxidase, *Biochemistry 42*, 5600−5608.
39. Carpena, X., Wiseman, B., Deemagarn, T., Singh, R., Switala, J., Ivancich, A., Fita, I., and Loewen, P. C. (2005) A molecular switch and electronic circuit modulate catalase activity in catalase-peroxidases, *EMBO Rep. 6*, 1156−1162.
40. Hersleth, H. P., Ryde, U., Rydberg, P., Gorbitz, C. H., and Andersson, K. K. (2006) Structures of the high-valent metal-ion haem-oxygen intermediates in peroxidases, oxygenases and catalases, *J. Inorg. Biochem. 100*, 460−476.
41. Derat, E., and Shaik, S. (2006) Two-state reactivity, electromerism, tautomerism, and "surprise" isomers in the formation of compound II of the enzyme horseradish peroxidase from the principal species, compound I, *J. Am. Chem. Soc. 128*, 8185−8198.
42. Zhao, X., Girotto, S., Yu, S., and Magliozzo, R. S. (2004) Evidence for radical formation at Tyr-353 in *Mycobacterium tuberculosis* catalase-peroxidase (KatG), *J. Biol. Chem. 279*, 7606−7612.
43. Sivaraja, M., Goodin, D. B., Smith, M., and Hoffman, B. M. (1989) Identification by ENDOR of Trp191 as the free-radical site in cytochrome c peroxidase compound ES, *Science 245*, 738−740.
44. Carpena, X., Wiseman, B., Deemagarn, T., Herguedas, B., Ivancich, A., Singh, R., Loewen, P. C., and Fita, I. (2006) Roles for Arg426 and Trp111 in the modulation of NADH oxidase activity of the catalase-peroxidase KatG from *Burkholderia pseudomallei* inferred from pH-induced structural changes, *Biochemistry 45*, 5171−5179.

BI062266+